Supporting information

Enhancing remarkable adsorption of Pb^{2+} in a series of sulfonic-functionalized Zr-based MOF: a combined theoretical and experimental study for elucidating adsorption mechanism

Cuong C. Tran,[a] Hieu C. Dong,[b,c] Vy T. N. Truong,[d] Thinh T. M. Bui,[a] Hung N. Nguyen,[a] Tuyet A. T. Nguyen,[a] Nam N. Dang[c] and My V. Nguyen*[,a]

[a]Faculty of Chemistry, Ho Chi Minh City University of Education, Ho Chi Minh City, 700000, Vietnam.

[b]Future Materials and Devices Laboratory, Institute of Fundamental and Applied Sciences, Duy Tan University, Ho Chi Minh City, 700000, Vietnam.

[c]Faculty of Natural Sciences, Duy Tan University, Da Nang, 550000, Vietnam.

[d]Royal Melbourne Institute of Technology (RMIT) University, Ho Chi Minh City 700000, Vietnam.

*To whom correspondence should be addressed: mynv@hcmue.edu.vn

Keywords: SO_3-functionalized Zr-MOFs, uptake of Pb^{2+}, Adsorption mechanism of heavy metal ion.

Table of Contents

Section S1. Synthesis of materials

Synthesis of Zr-bcu-NDC

A mixture of $ZrOCl_2 \cdot 8H_2O$ (400 mg, 1.246 mmol) and H_2NDC (130 mg, 0.602 mmol) was introduced into a 20 mL Pyrex vial containing DMF (5 mL) and trifluoroacetic acid (1.1 mL). The mixture was then ultrasonicated in 5 min and heated at 120 ^oC for 3 days. Continuously, the solid was centrifugated, washed with DMF for 2 days (20 mL per day), and exchanged with MeOH for 2 days (20 mL per day). Finally, the sample was collected, dried, and activated under vacuum at 80 ^oC for 12 h to obtain a white powder.

Synthesis of acidified VNU-17 ($H^+ \subset$VNU-17)

A mixture of $ZrOCl_2 \cdot 8H_2O$ (260 mg, 0.810 mmol) and H_3SNDC (270 mg, 0.915 mmol) was added to a 100 mL glass bottle including 40 mL of DMF and 6.5 mL formic acid. Then, the mixture was ultrasonicated in 10 min and heated for 2 days at 120 ^oC. The mixture was cooled to room temperature and centrifugated to acquire a white powder, termed pristine VNU-17 (DMA$\subset$VNU-17). This solid was washed with DMF for 3 days (15 mL per day) to remove the unreacted substances and immersed in a H_2SO_4 solution of 0.3 M for 2 days (5 times per day). Subsequently, the sample was washed with an excess amount of methanol and water solution to pH = 5. The material was exchanged with MeOH for 2 days (20 mL per day), dried, and activated under vacuum at 80 ^oC for 12 h to acquire a pure solid, namely $H^+ \subset$VNU-17.

Synthesis of acidified VNU-23 ($H^+ \subset$VNU-23)

$ZrOCl_2 \cdot 8H_2O$ (196 mg, 0.611 mmol) and H_4SNDC (248 mg, 0.660 mmol) was dissolved by a mixture containing 30 mL of DMF and 7.5 mL formic acid in a 100 mL glass bottle. The mixture was then heated at 120 ^oC for 2 days. After cooling down to room temperature, the white solid was centrifugated, namely pristine VNU-23 (DMA$\subset$VNU-23). This solid was washed with DMF for 3 days (15 mL per day) to remove the unreacted starting materials and immersed in a 0.3 M of H_2SO_4 solution for 2 days (5 times per day). Next, the product was washed with an excess amount of methanol and water solution to pH = 5. Finally, the product was exchanged with MeOH for 2 days (20 mL per day), dried, and activated under vacuum at 80 ^oC for 12 h to acquire a pure solid, termed $H^+ \subset$VNU-23.

Section S2. ^{1}H-NMR analysis of H_3SNDC, H_4SNDC, digested $H^+\subset$VNU-17, and digested $H^+\subset$VNU-23

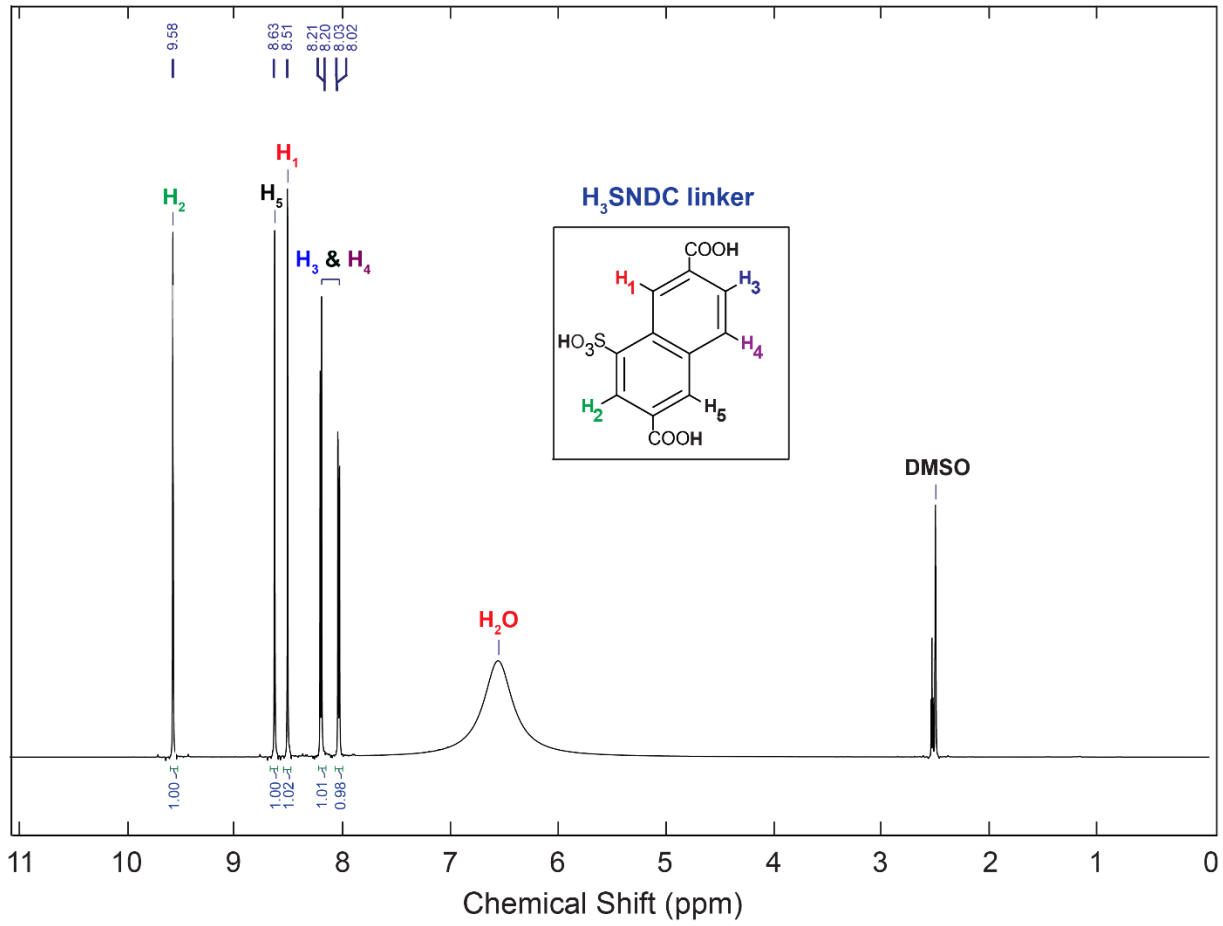

Figure S1. ^{1}H-NMR analysis of the H_3SNDC linker.

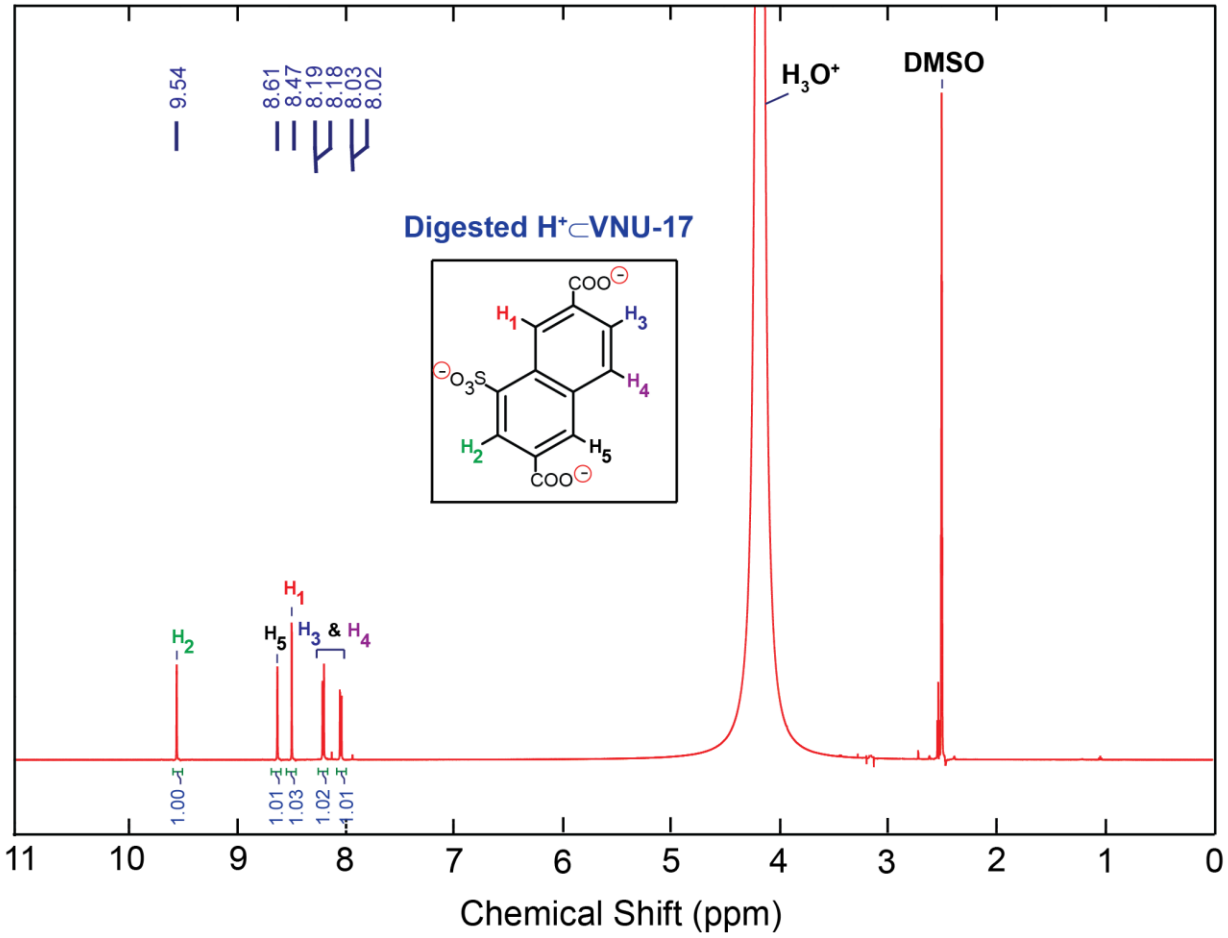

Figure S2. ^{1}H-NMR analysis of digested H^{+}⊂VNU-17.

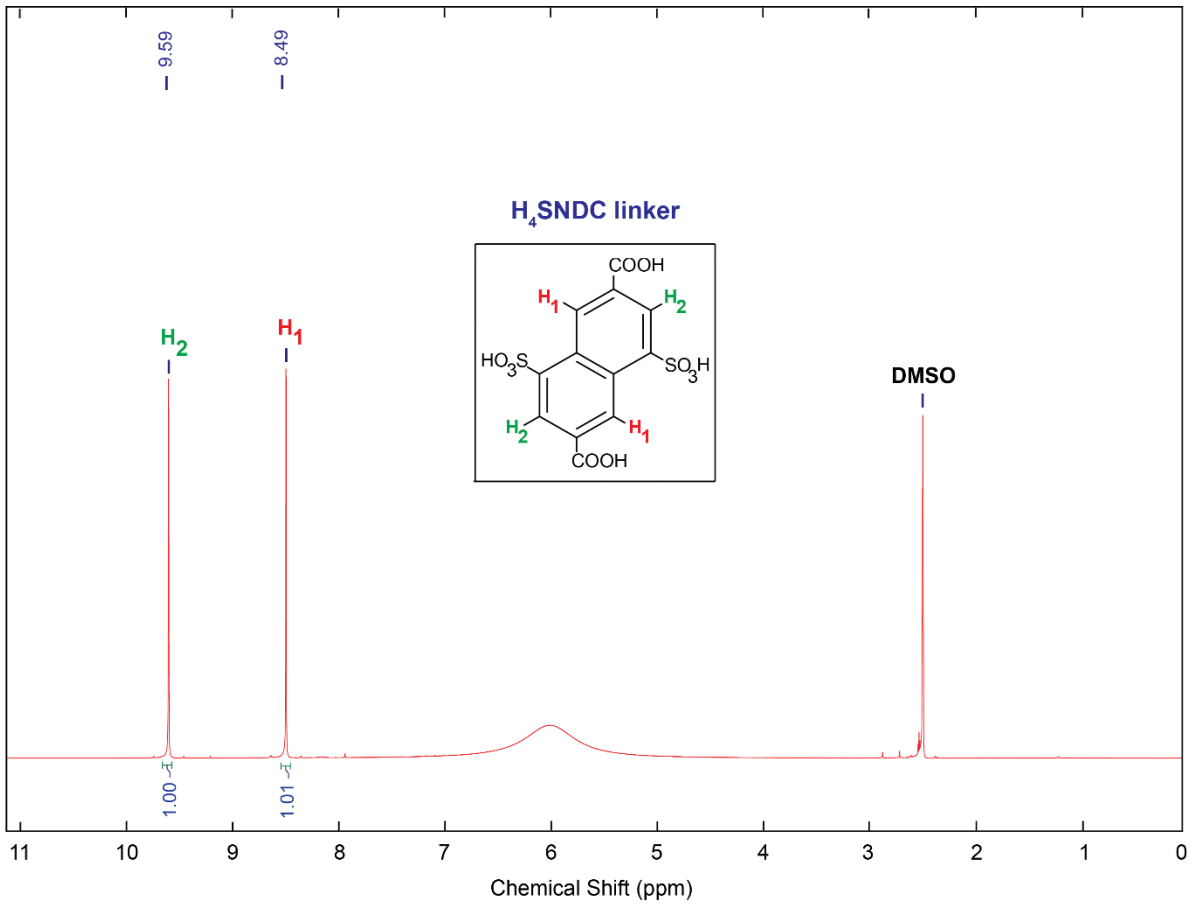

Figure S3. ^{1}H-NMR analysis of the H_4SNDC linker.

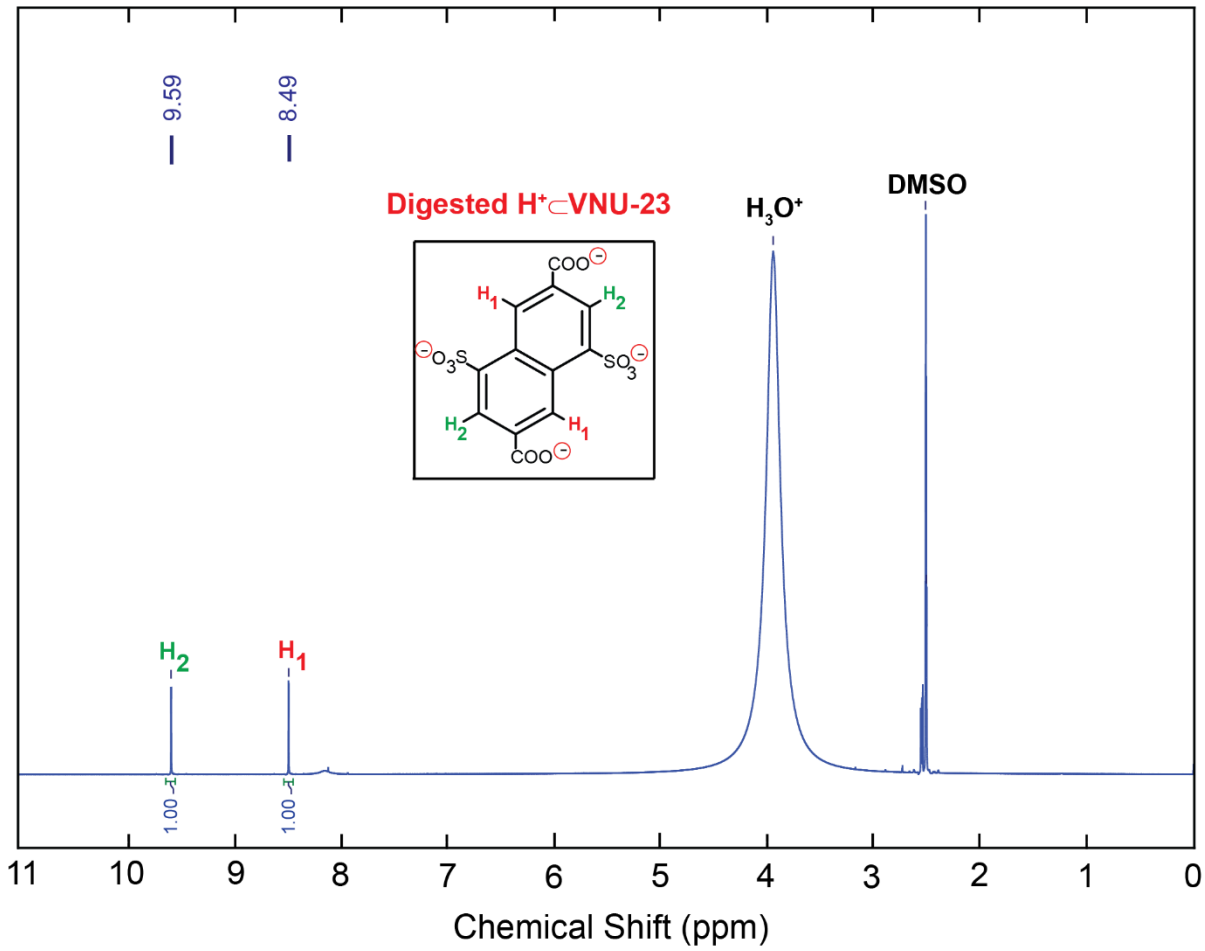

Figure S4. ^{1}H-NMR analysis of digested $H^{+}\subset$VNU-23.

Section S3. Fourier transform infrared (FT-IR) analysis

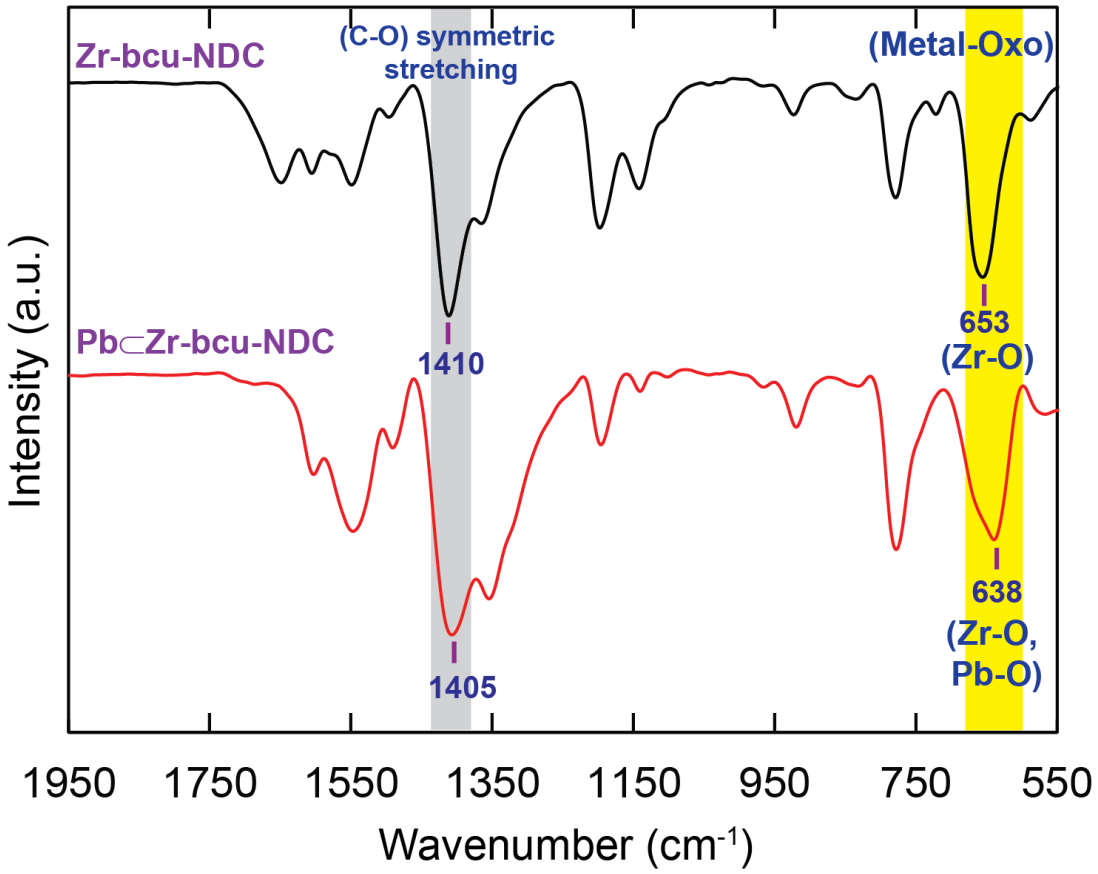

Figure S5. FT-IR spectrum of Zr-bcu-NDC (black) in comparison with Pb⊂Zr-bcu-NDC (red).

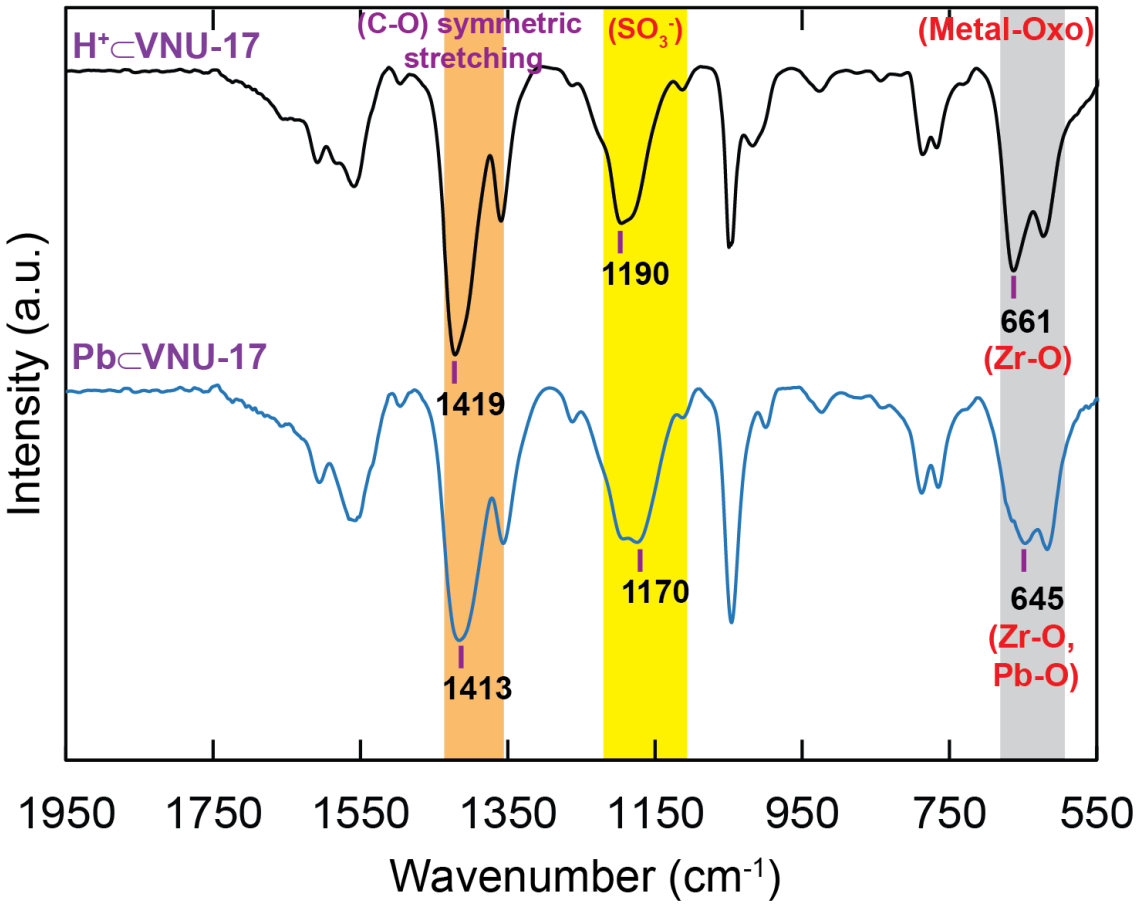

Figure S6. FT-IR spectrum of H^+⊂VNU-17 (black) in comparison with Pb⊂VNU-17 (blue).

Section S4. Powder X-ray diffraction patterns (PXRD)

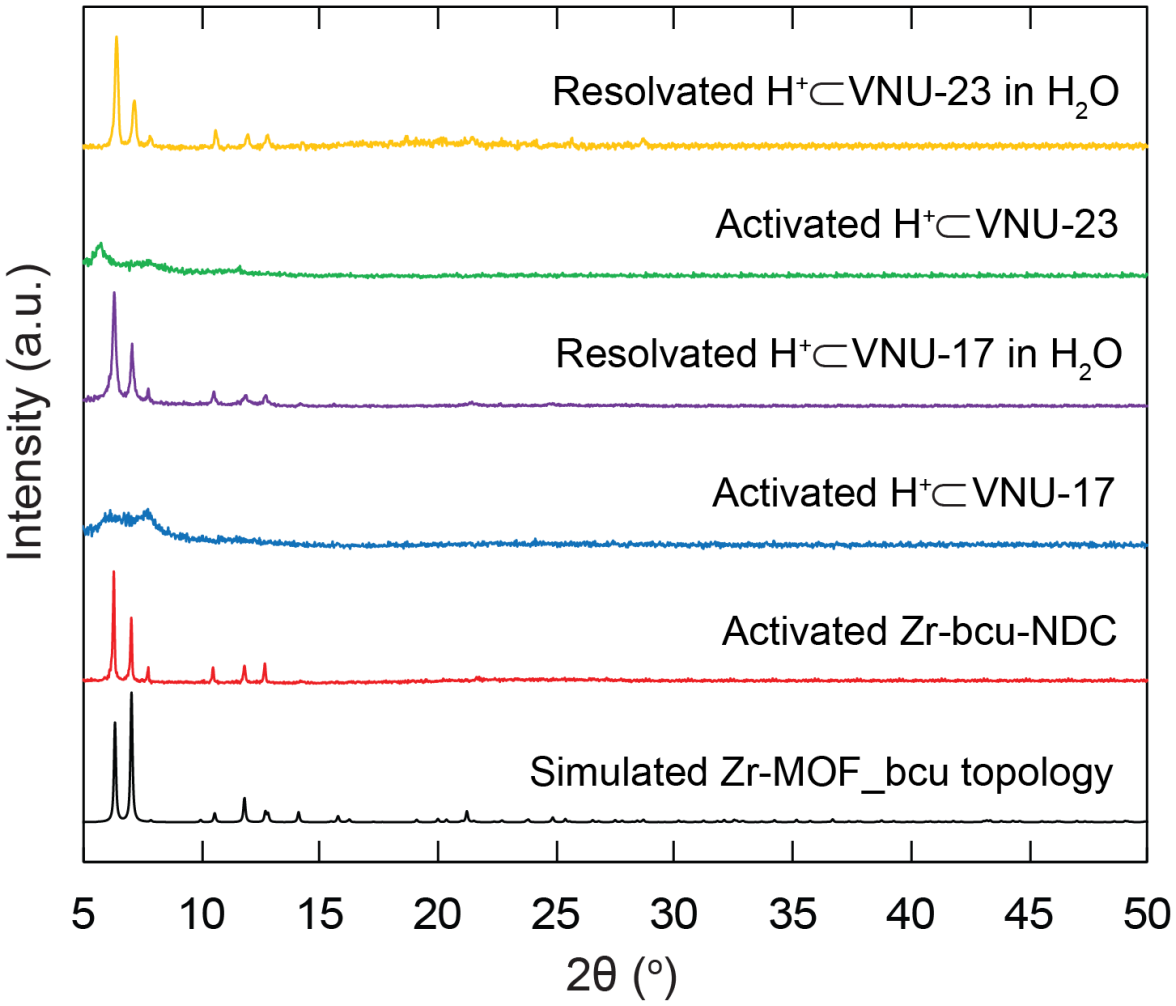

Figure S7. PXRD patterns of simulated structure with bcu topology (black) in comparison with activated Zr-bcu-NDC (red), activated H^+⊂VNU-17 (blue), re-solvated H^+⊂VNU-17 in water (purple), activated H^+⊂VNU-23 (green), and re-solvated H^+⊂VNU-23 in water (orange).

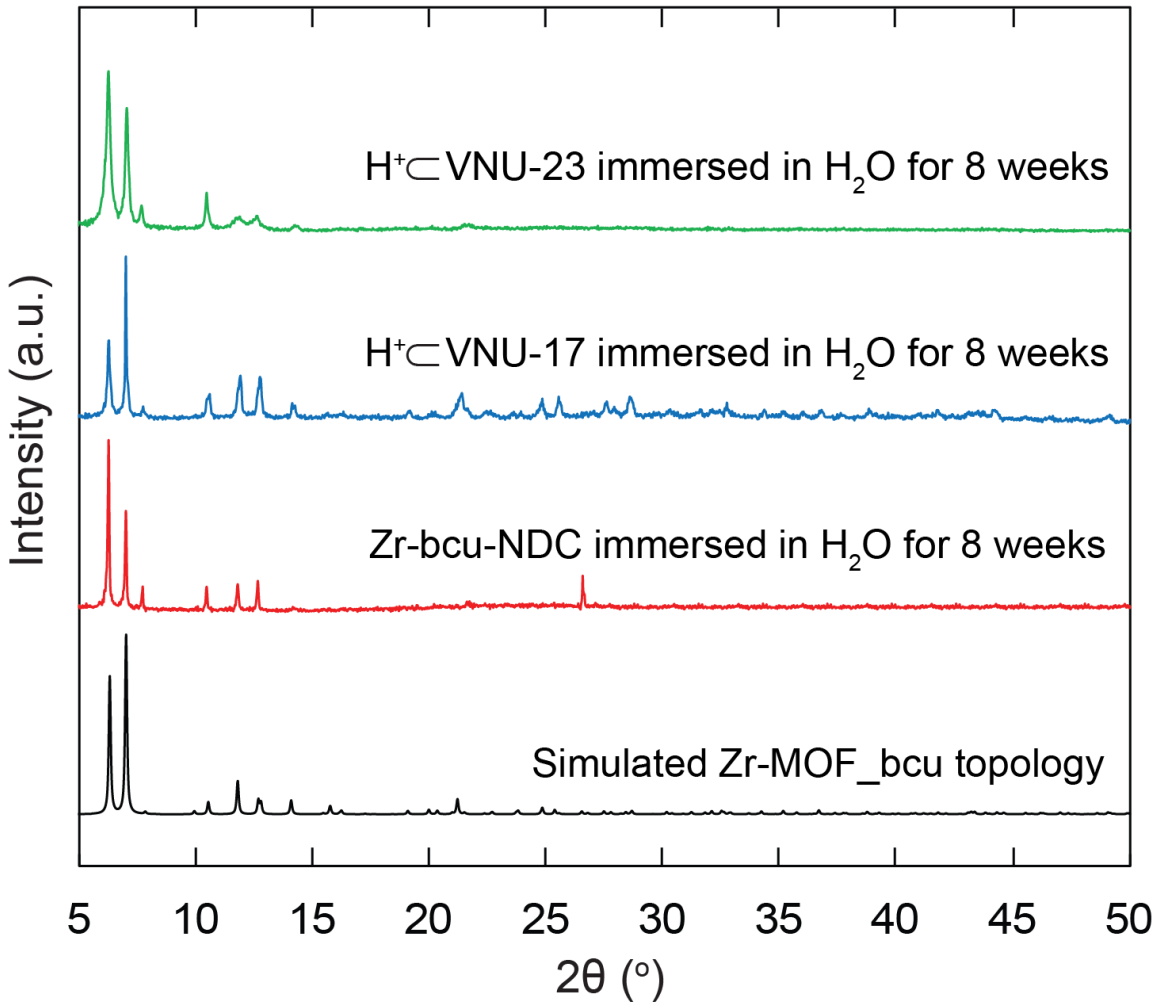

Figure S8. PXRD patterns of simulated structure with bcu topology (black) in comparison with the materials immersed in water for 8 weeks such as Zr-bcu-NDC (red), $H^+\subset$VNU-17 (blue), and $H^+\subset$VNU-23 (green).

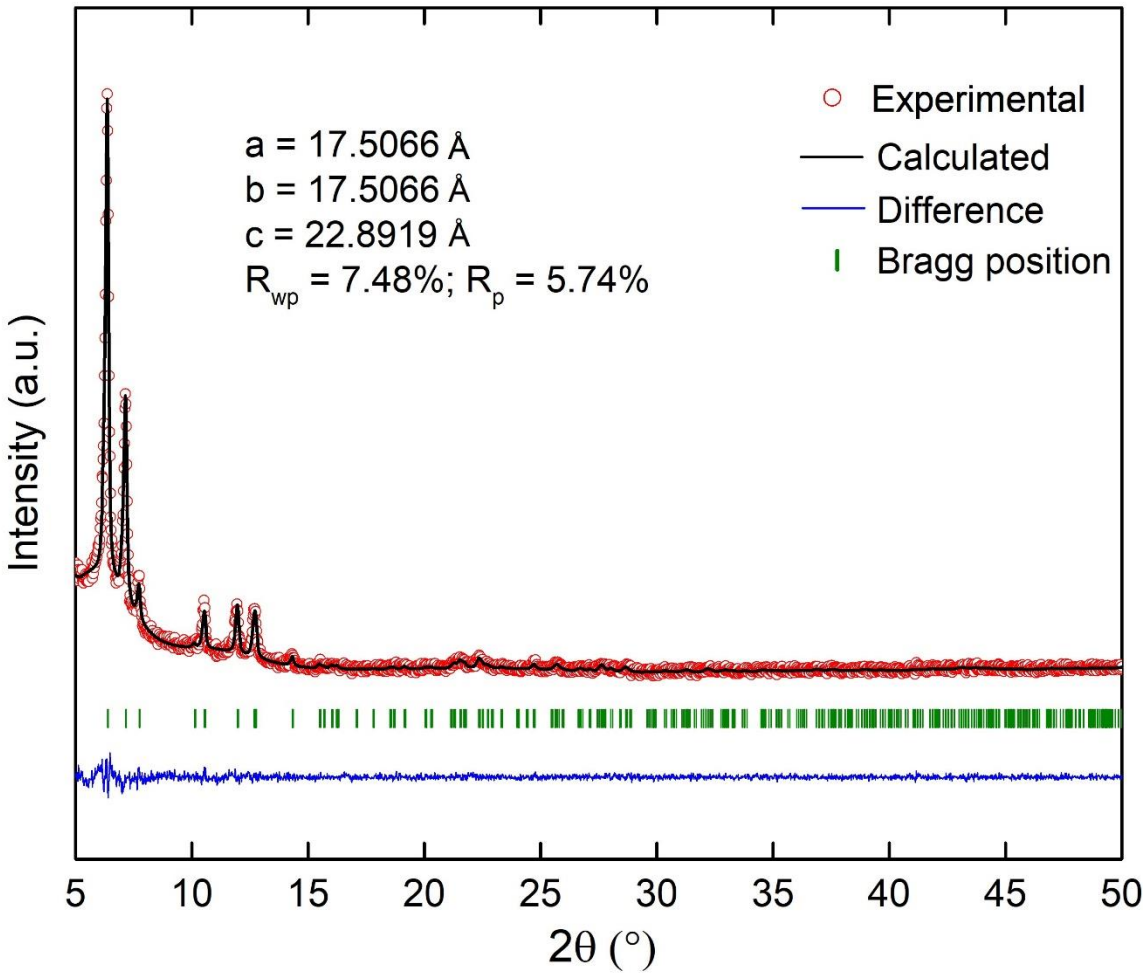

Figure S9. The Rietveld refinements using P_1 space group of Pb⊂VNU-23: The experimental (red), calculated (black), and difference (blue) patterns. The Bragg positions are marked as green bars.

Section S5. Thermogravimetric analysis (TGA) and Differential scanning calorimetry (DSC) curves

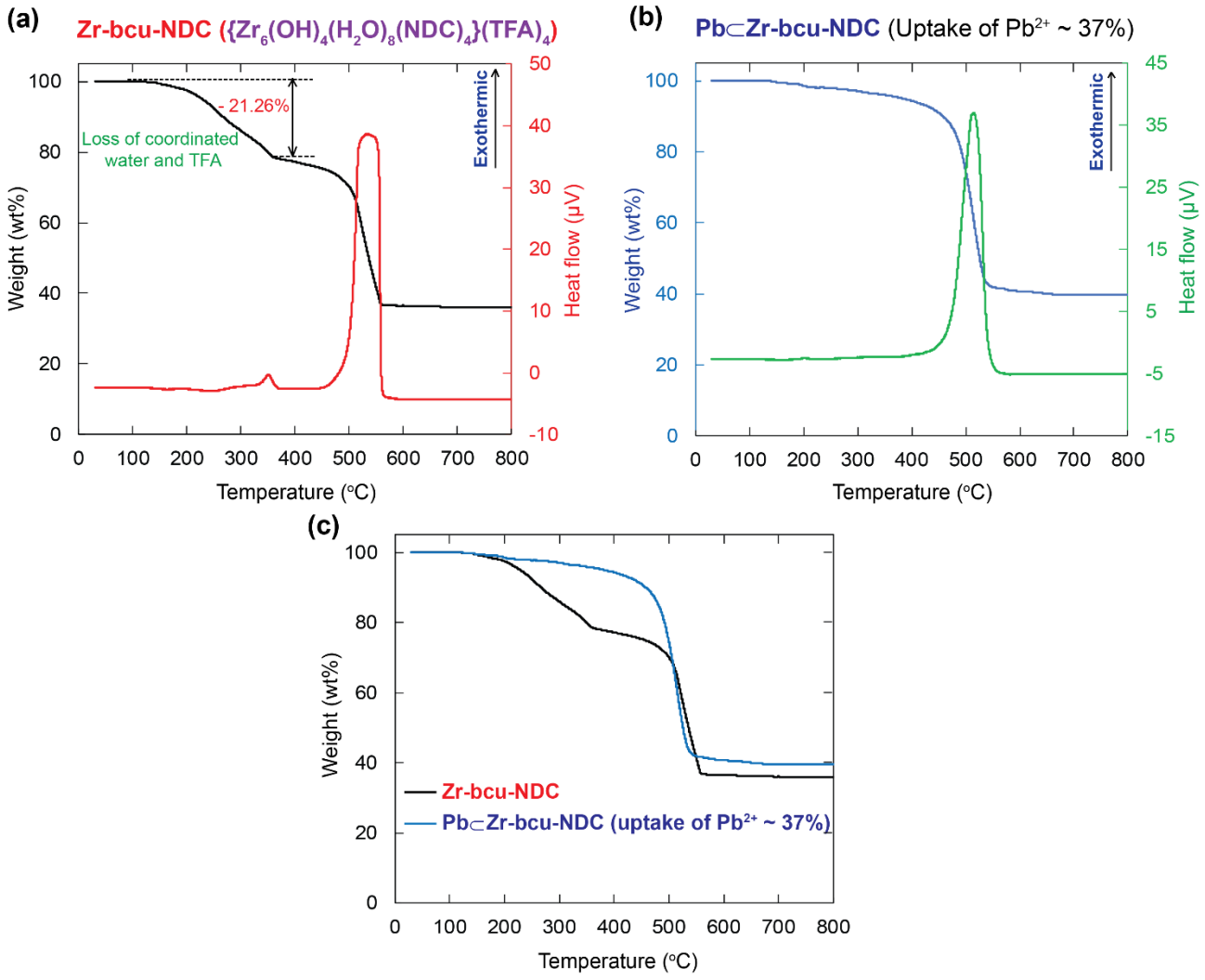

Figure S10. TGA-DSC curves of Zr-bcu-NDC (a), and Pb⊂Zr-bcu-NDC (b). TGA curves of Zr-bcu-NDC (black) in comparison with Pb⊂Zr-bcu-NDC (blue) (c). Herein, Pb⊂Zr-bcu-NDC sample was collected after adsorption of Pb^{2+} (20 mg L^{-1}) onto Zr-bcu-NDC in 24 h with maximum uptake of Pb^{2+} about 37%.

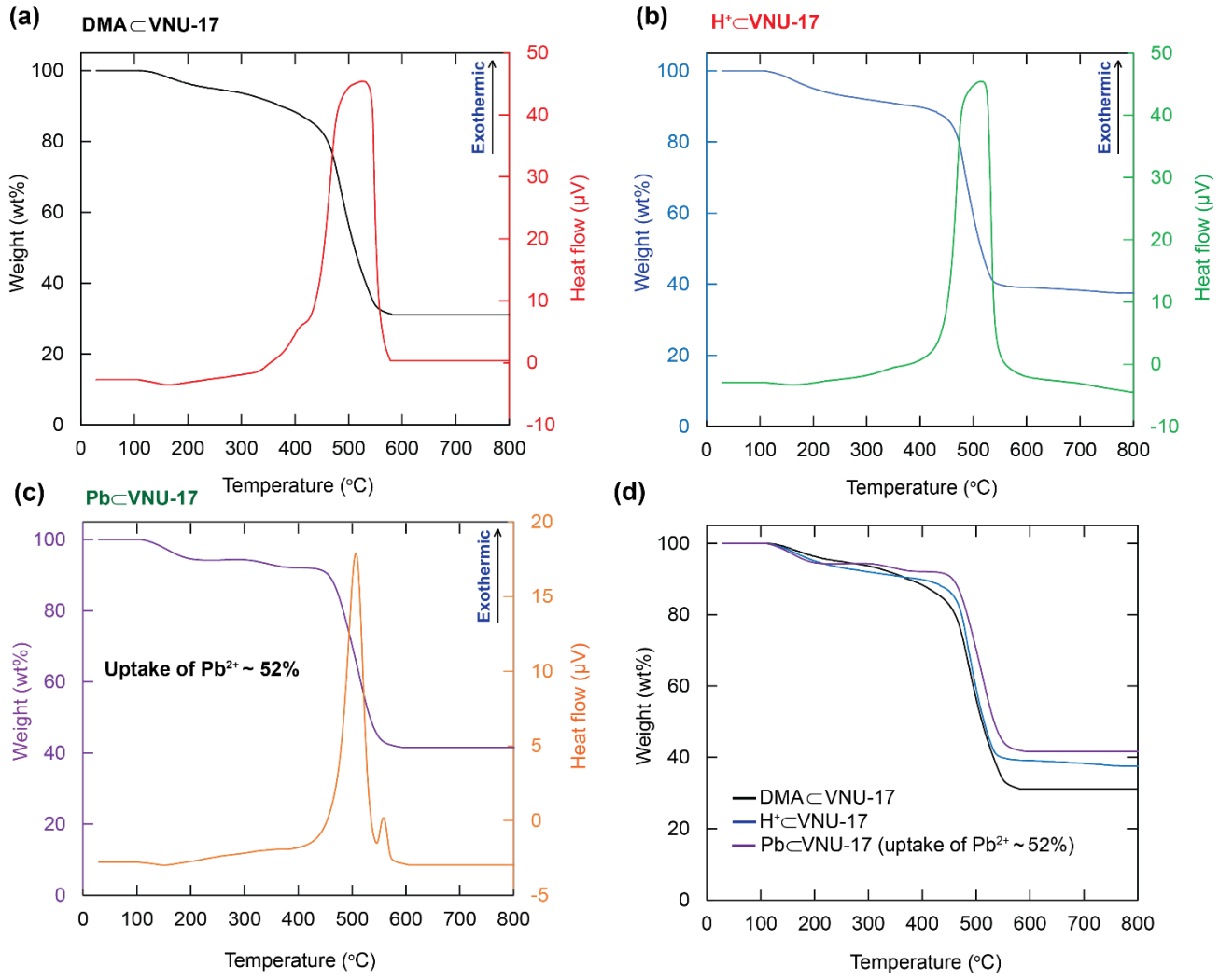

Figure S11. TGA-DSC curves of DMA⊂VNU-17 (a), H^+⊂VNU-17 (b), and Pb⊂VNU-17 (c). TGA curves of DMA⊂VNU-17 (black) in comparison with H^+⊂VNU-17 (blue), and Pb⊂VNU-17 (purple) (d). Herein, Pb⊂VNU-17 sample was obtained after adsorption of Pb^{2+} (20 mg L^{-1}) onto H^+⊂VNU-17 in 24 h with maximum uptake of Pb^{2+} about 52%.

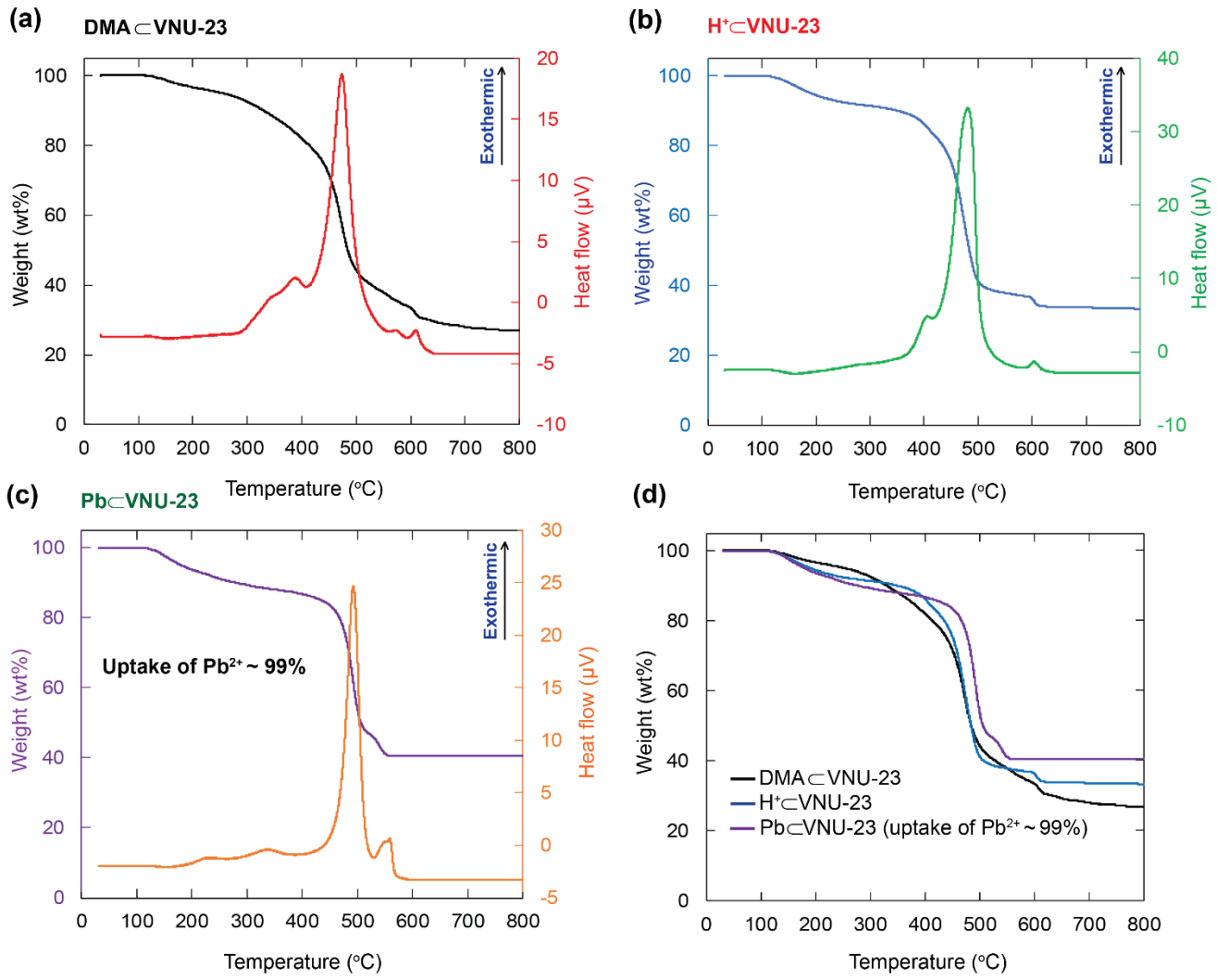

Figure S12. TGA-DSC curves of DMA⊂VNU-23 (a), H^+⊂VNU-23 (b), and Pb⊂VNU-23 (c). TGA curves of DMA⊂VNU-23 (black) in comparison with H^+⊂VNU-23 (blue), and Pb⊂VNU-23 (purple) (d). Herein, Pb⊂VNU-23 sample was obtained after adsorption of Pb^{2+} (20 mg L^{-1}) onto H^+⊂VNU-23 in 24 h with maximum uptake of Pb^{2+} about 99%.

Section S6. N_2 adsorption measurement

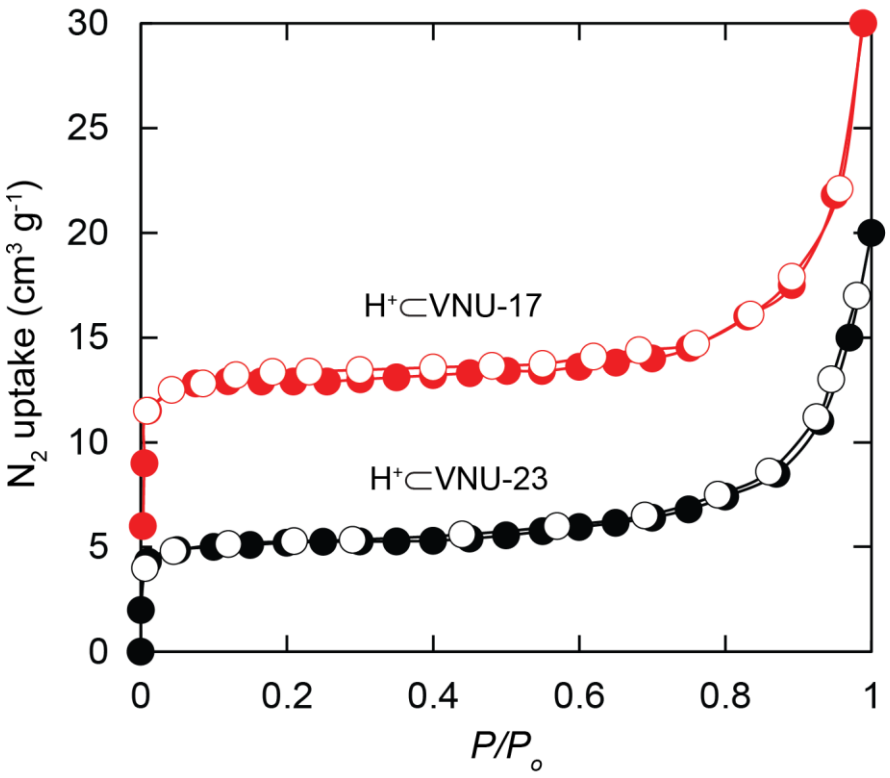

Figure S13. N_2 isotherm of H^+⊂VNU-17 (red) and H^+⊂VNU-23 (black) at 77K. The closed and open circles symbolize the adsorption and desorption branches of the isotherm, respectively.

Section S7. Scanning electron microscopy (SEM) and energy-dispersive X-ray mapping (EDX-mapping) analysis

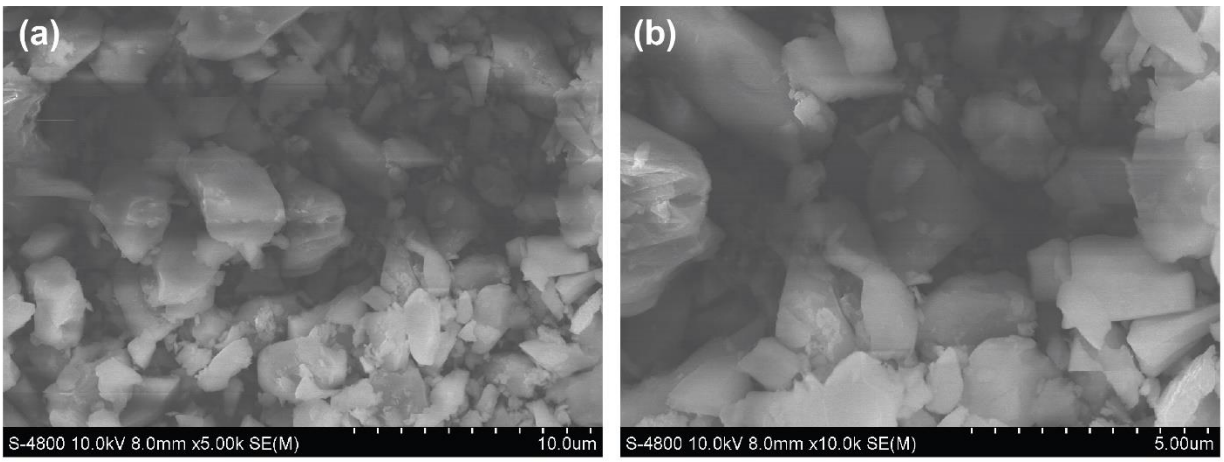

Figure S14. SEM images of Zr-bcu-NDC at different scale bars of 10.0 μm, and 5.00 μm, respectively.

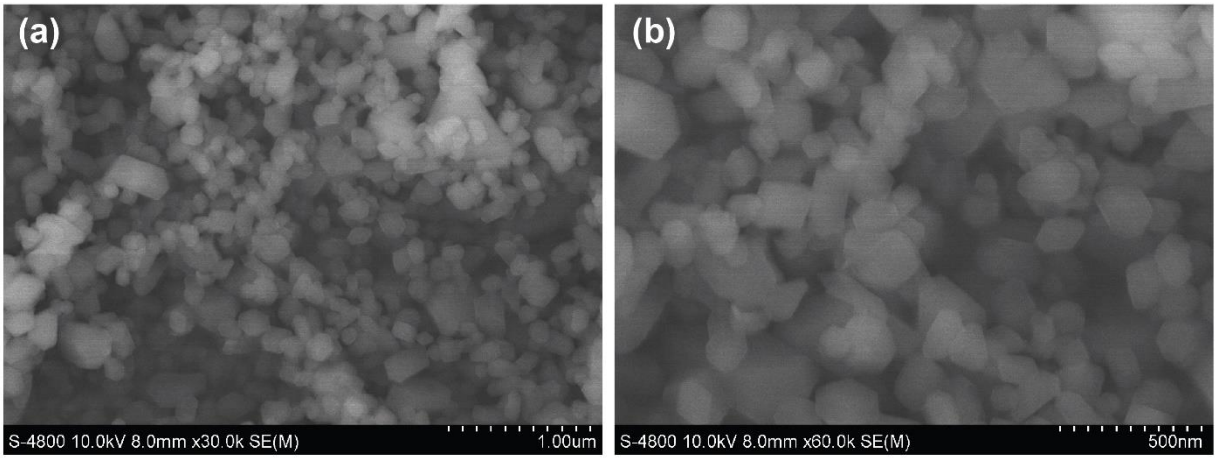

Figure S15. SEM images of $H^+ \subset$VNU-17 at different scale bars of 1.00 μm, and 500 nm, respectively.

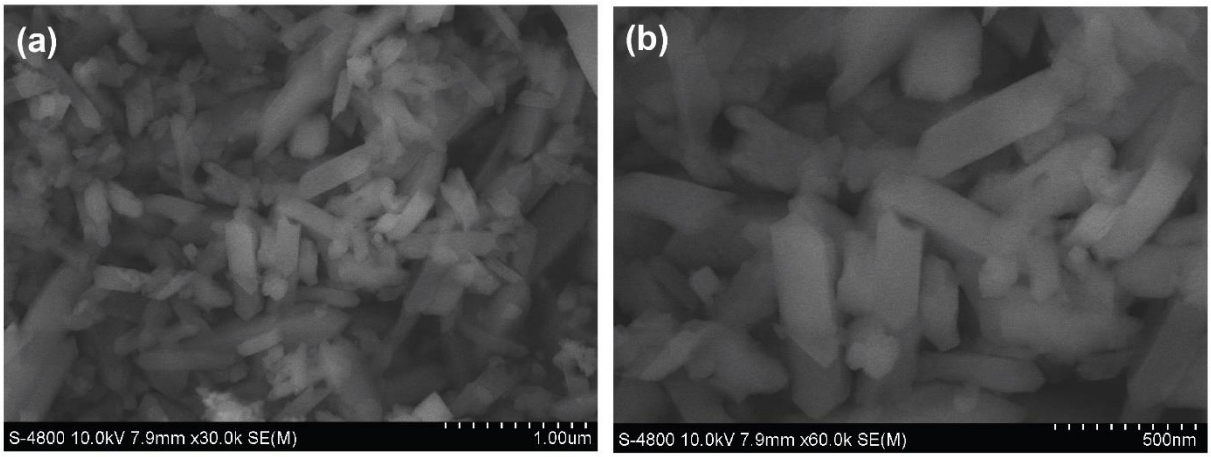

Figure S16. SEM images of $H^+ \subset$VNU-23 at different scale bars of 1.00 μm, and 500 nm, respectively.

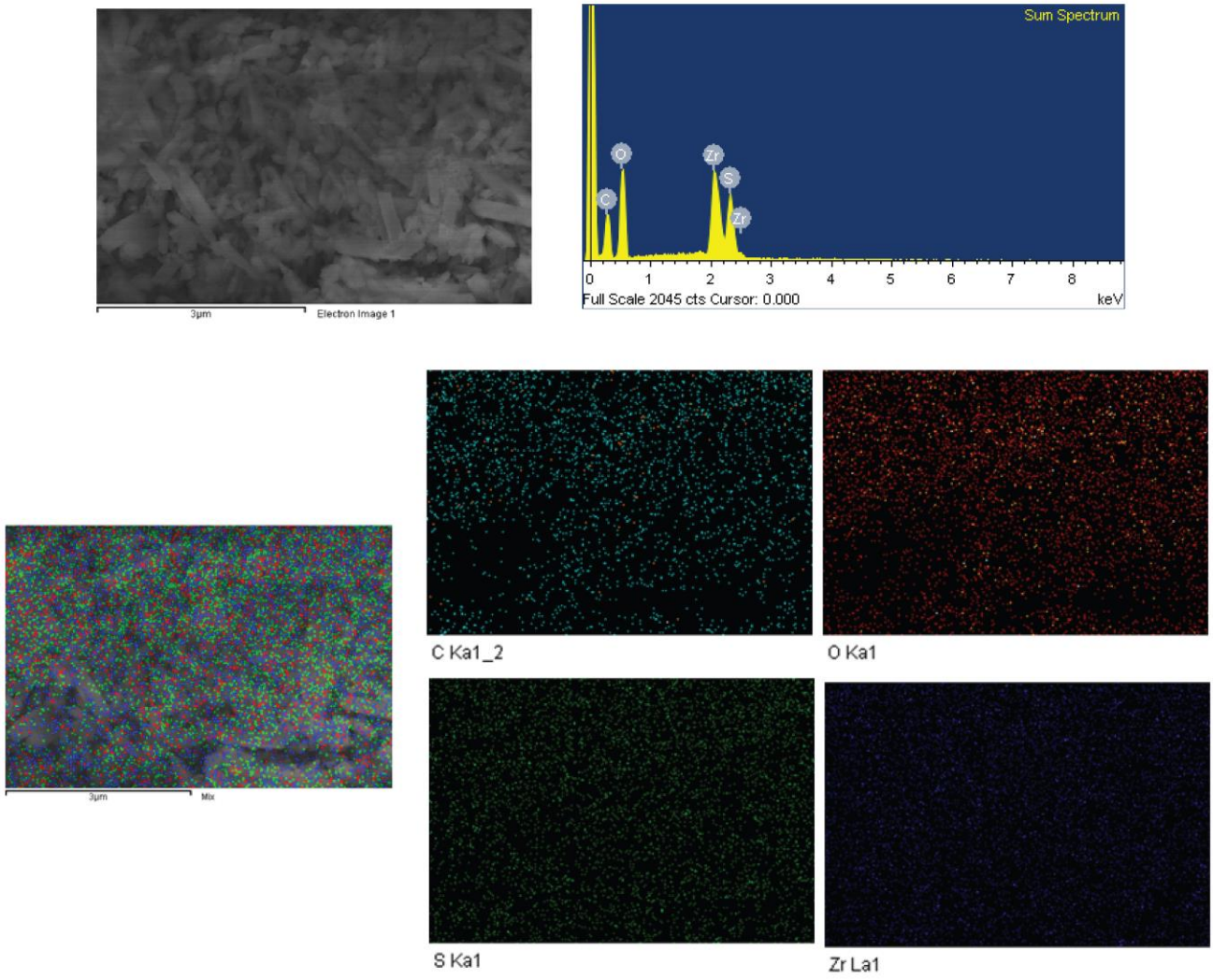

Figure S17. Elemental mapping by SEM-EDX of $H^+ \subset$VNU-23.

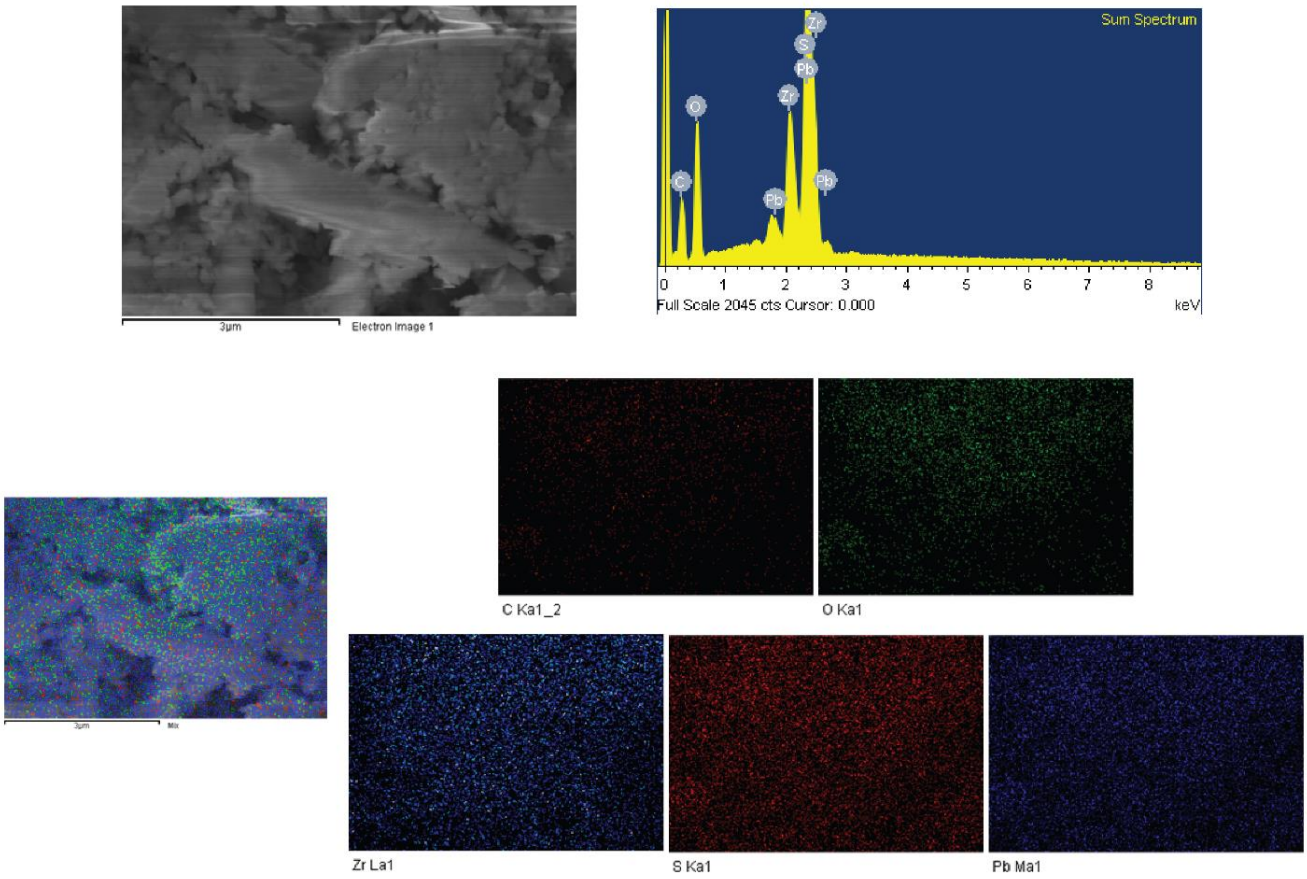

Figure S18. Elemental mapping by SEM-EDX of Pb⊂VNU-23 (uptake of Pb^{2+} ~ 99%).

Section S8. Transmission electron microscopy (TEM) analysis

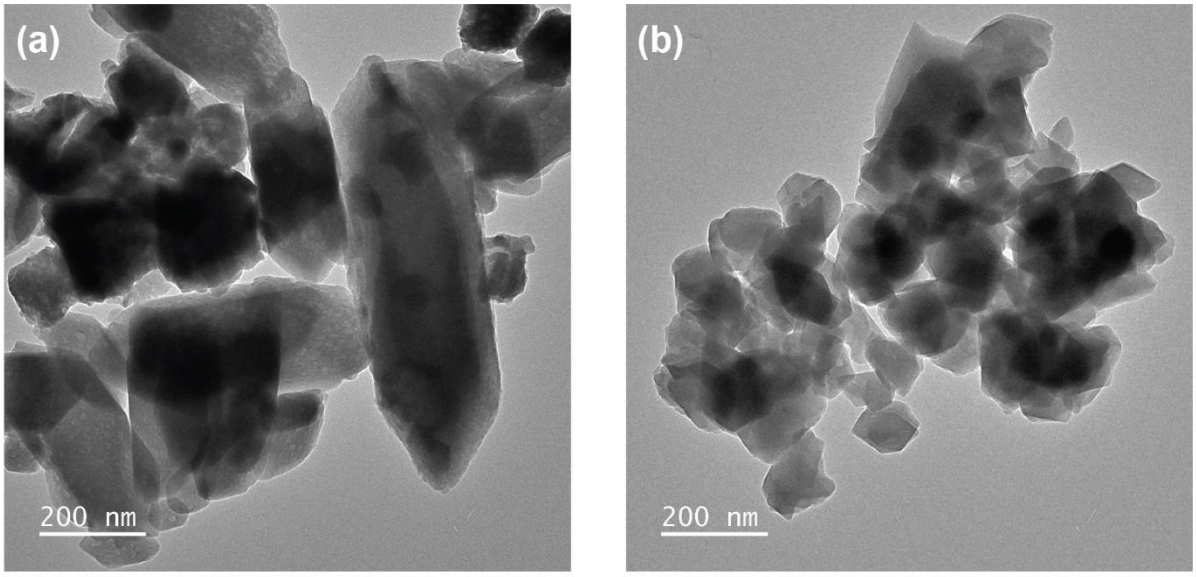

Figure S19. TEM images of $H^{+}\subset$VNU-23 before adsorption of Pb^{2+} (a) and after recycling (b) at scale bar of 200 nm.

Section S9. Adsorption studies

Adsorption isotherms

The four adsorption isotherm models of Langmuir, Freundlich, Temkin, and Dubinin-Radushkevich are displayed in the equations (1), (2), (3), and (4):

$$q_e = \frac{q_m.K_L.C_e}{1+K_L.C_e} \quad (1)$$

$$q_e = K_F.C_e^{1/n} \quad (2)$$

$$q_e = \frac{RT}{b}\ln(k_T C_e) \quad (3)$$

$$q_e = q_m.e^{-K_{DR}.\varepsilon^2} \quad (4)$$

Where C_e (mg L^{-1}) and q_e (mg g^{-1}) are the Pb^{2+} concentration and adsorption capacity at equilibrium, respectively, q_m (mg g^{-1}) is the theoretical maximum capacity of the Pb^{2+} adsorption. K_L (L mg^{-1}), K_F (mg g^{-1} (L $g^{-1})^{1/n}$), K_T (L mg^{-1}), and K_{DR} (mg g^{-1}) symbolize the constants of Langmuir, Freundlich, Temkin, and Dubinin-Radushkevich models, respectively. 1/n value illustrates the adsorption capacity index of Freundlich isotherm. b, R, T are the constant of adsorption heat, gas, and temperature in Kelvin, respectively. ε is a constant.

The separation factor R_L is also employed by eqn (5):

$$R_L = \frac{1}{1+K_L C_o} \quad (5)$$

Where C_o and K_L are the initial concentration of Pb^{2+} and the constant of Langmuir, respectively.

Adsorption kinetics

The pseudo first order, pseudo second order, and intra-particle diffusion models obey the equations (6), (7), and (8):

$$q_t = q_e.(1 - e^{-k_1 t}) \quad (6)$$

$$\frac{t}{q_t} = \frac{1}{k_2 q_e^2} + \frac{t}{q_e} \quad (7)$$

$$q_t = k_i t^{1/2} + c \quad (8)$$

Where q_t (mg g^{-1}) and q_e (mg g^{-1}) are the Pb^{2+} uptake amounts at t and equilibrium time, respectively. k_1 (min^{-1}), k_2 (g mg^{-1} min^{-1}), and k_i (g mg^{-1} min^{-1}) are the rate constants of pseudo first order, pseudo second order, and intra-particle diffusion models, and c is the constant indicating the thickness of the boundary layer.

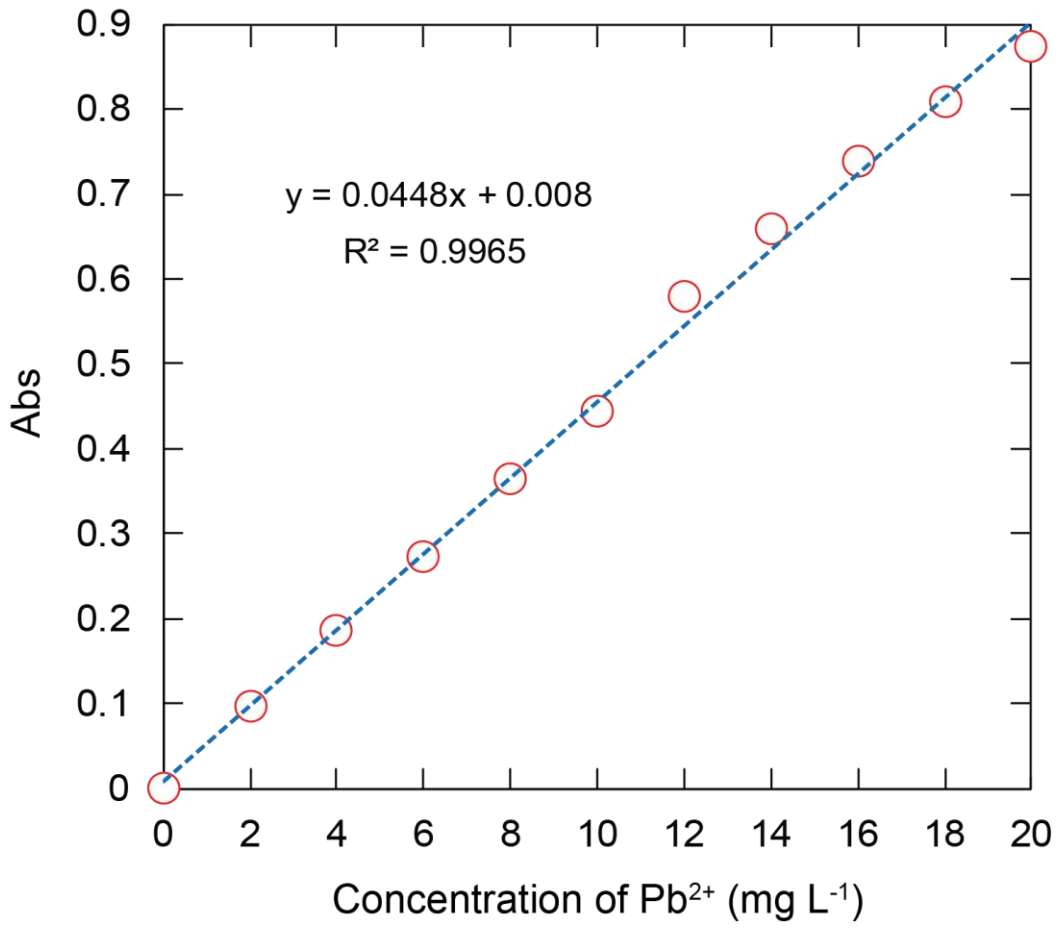

Figure S20. The relationship between the absorbed intensity (red dots) of Pb^{2+} and different concentrations of 0 - 20 mg L^{-1} by linear fitting.

The adsorption of Pb^{2+} onto $H^{+}\subset$VNU-17

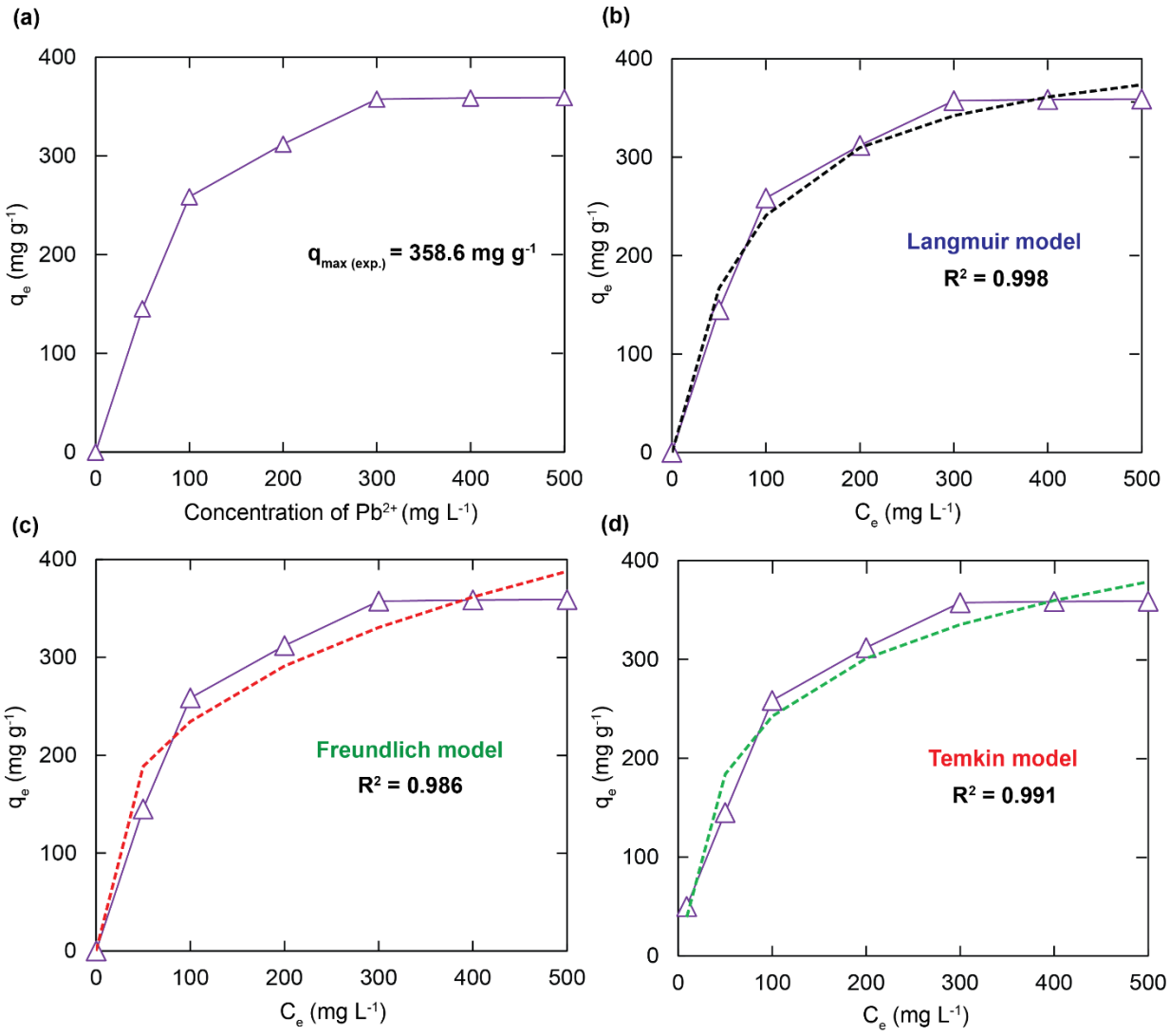

Figure S21. Effect of initial concentration on the adsorption capacity of Pb^{2+} onto $H^{+}\subset$VNU-17 [m = 30 mg, V = 100 mL, C_o: 50 - 500 mg L^{-1}, pH = 5.5, t = 24 h] (a). Data fitting with the adsorption isotherm models: Langmuir (b), Freundlich (c), Temkin (d).

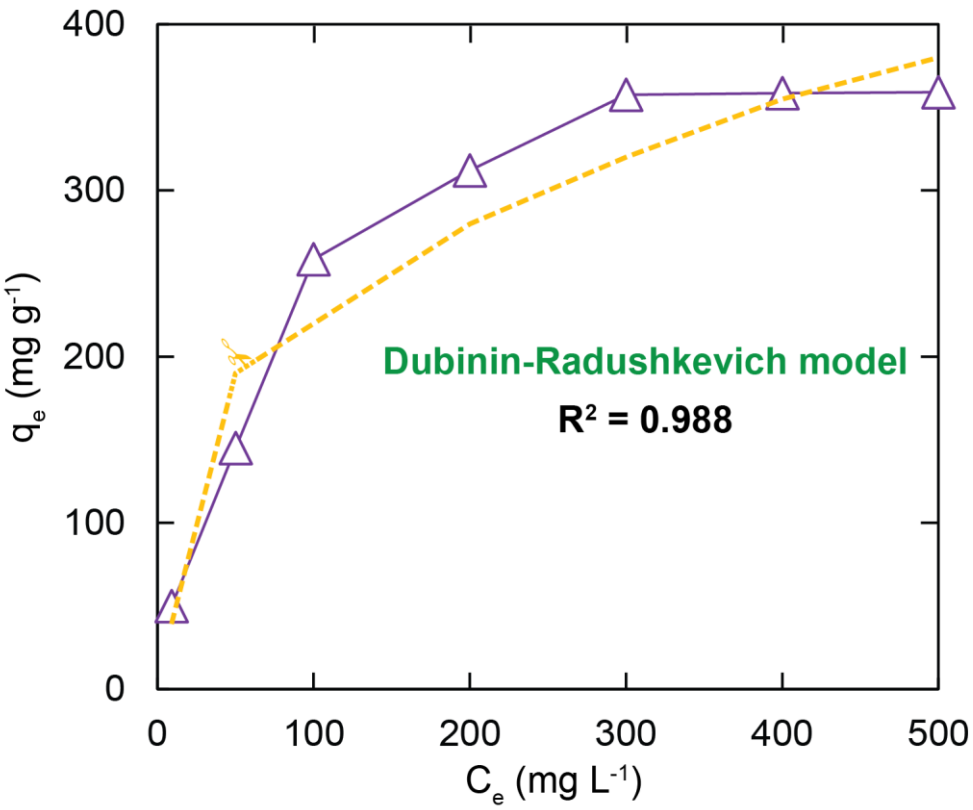

Figure S22. Data fitting with the Dubinin-Radushkevich adsorption isotherm model of the Pb^{2+} adsorption onto H^+⊂VNU-17.

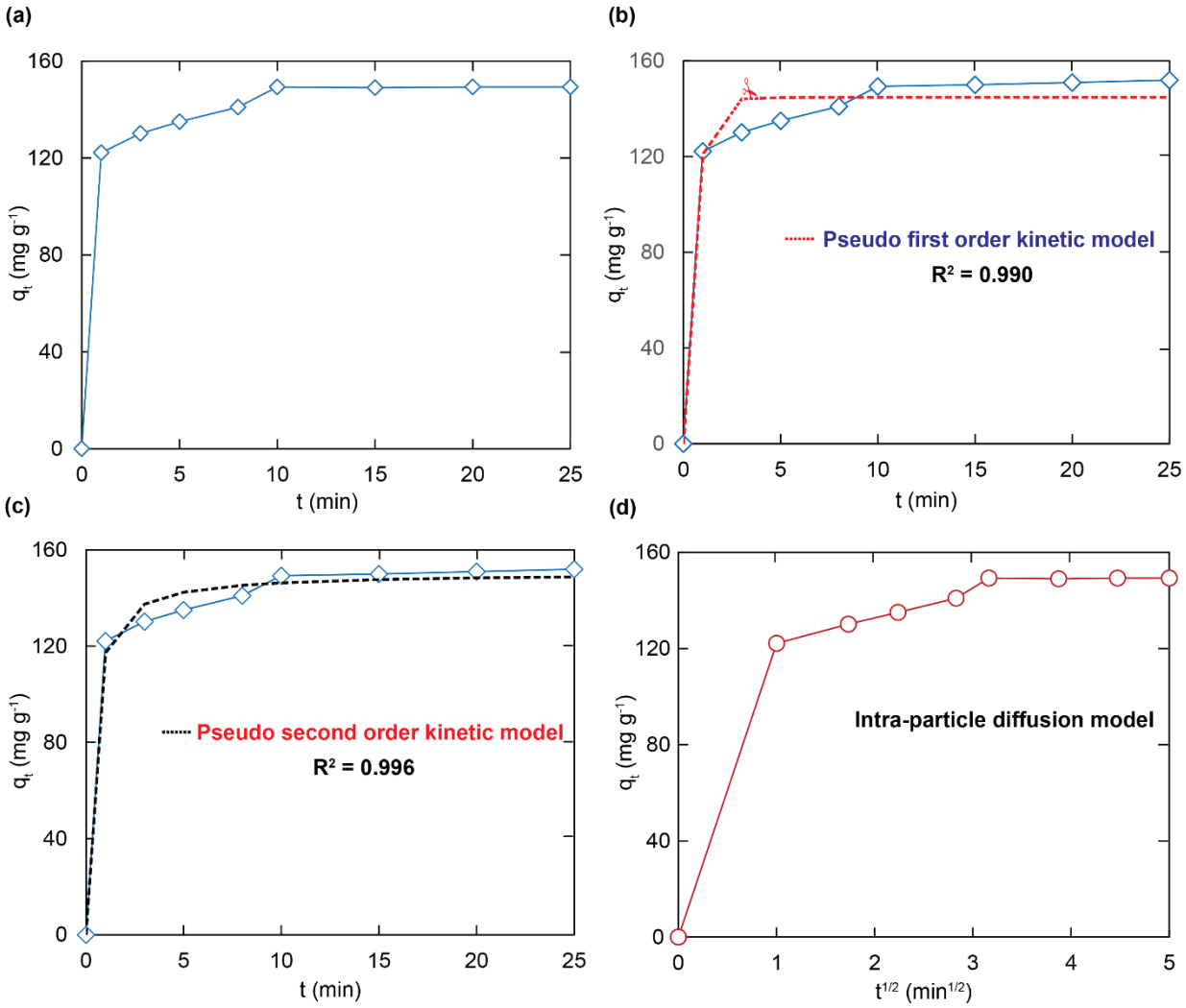

Figure S23. The kinetic curve for the adsorption of Pb^{2+} on $H^+\subset$VNU-17 [m = 5 mg, V = 50 mL, C_o = 40 mg L^{-1}, pH = 5] (a). Data fitting with the adsorption kinetic models: pseudo first order (b), pseudo second order (c), and intra-particle diffusion model (d).

The adsorption of Pb^{2+} onto $H^{+}\subset$VNU-23

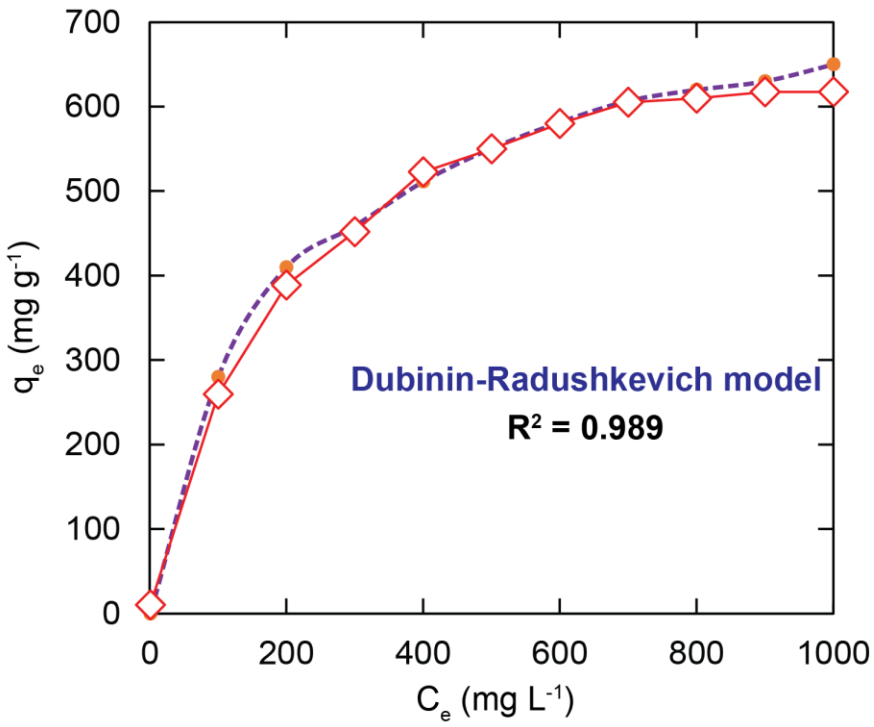

Figure S24. Data fitting with the Dubinin-Radushkevich adsorption isotherm model of the Pb^{2+} adsorption onto $H^{+}\subset$VNU-23.

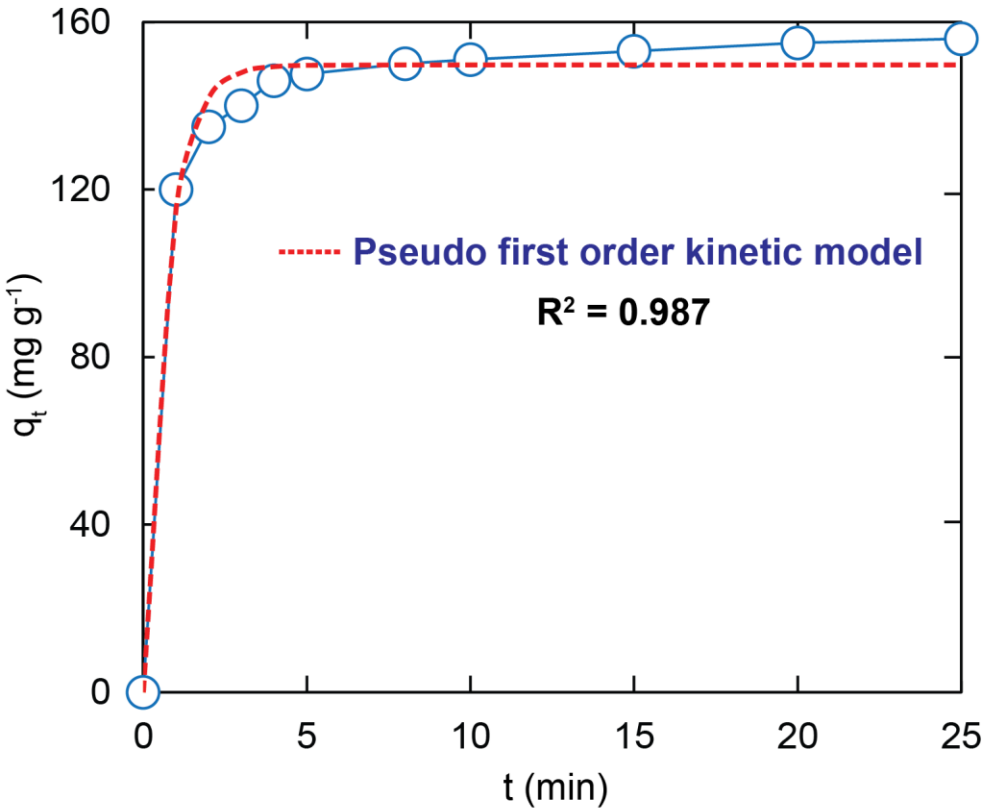

Figure S25. Data fitting with the pseudo first order kinetic model of the Pb^{2+} adsorption onto H^+⊂VNU-23.

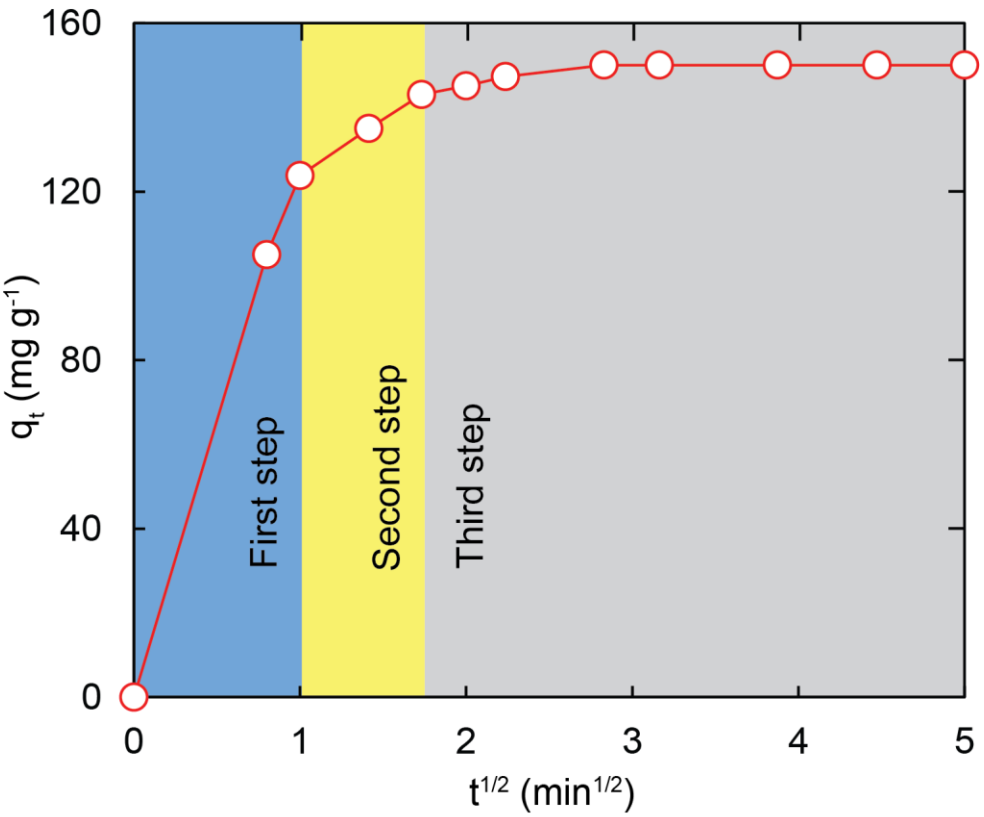

Figure S26. Data fitting with the intra-particle diffusion model of the Pb^{2+} adsorption onto H^+⊂VNU-23.

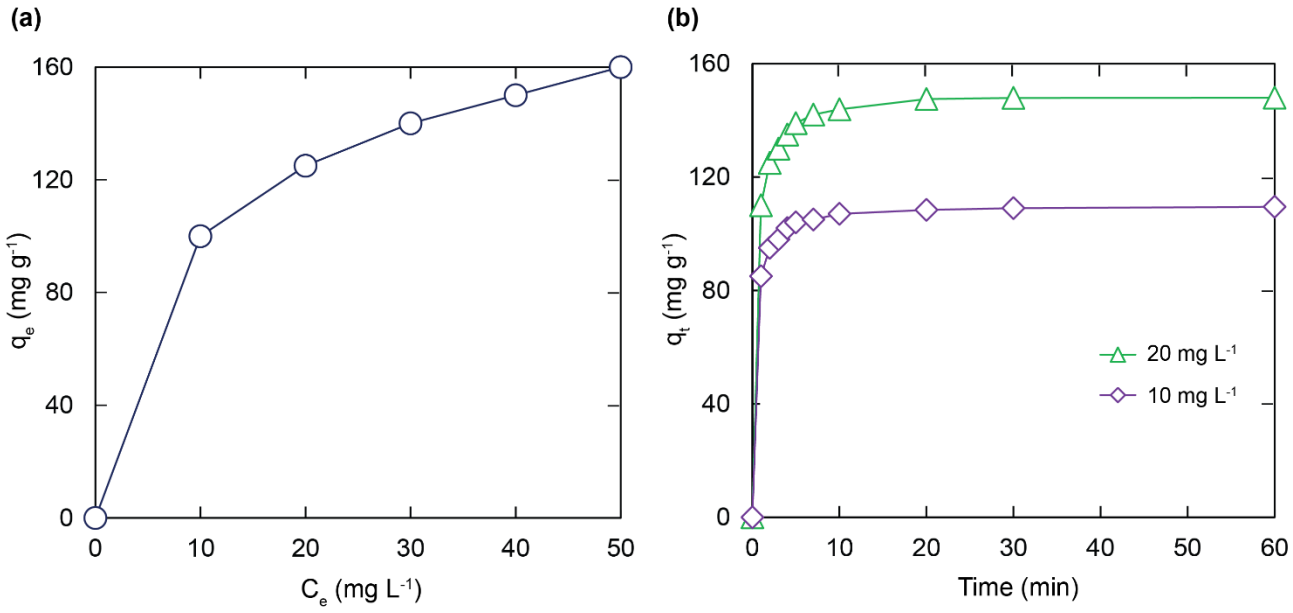

Figure S27. (a) Effect of low initial concentrations on the adsorption capacity of Pb^{2+} onto $H^{+}\subset$VNU-23 [m = 30 mg, V = 100 mL, Co: 10 - 50 mg L^{-1}, pH = 5.5, t = 24 h]; (b) The kinetic curve for the adsorption of Pb^{2+} at low concentrations onto $H^{+}\subset$VNU-23 [m = 5 mg, V = 50 mL, C_o = 10 mg L^{-1} and 10 mg L^{-1}, pH = 5].

Section S10. The stability of VNU-23 during the adsorption and desorption process of Pb^{2+}

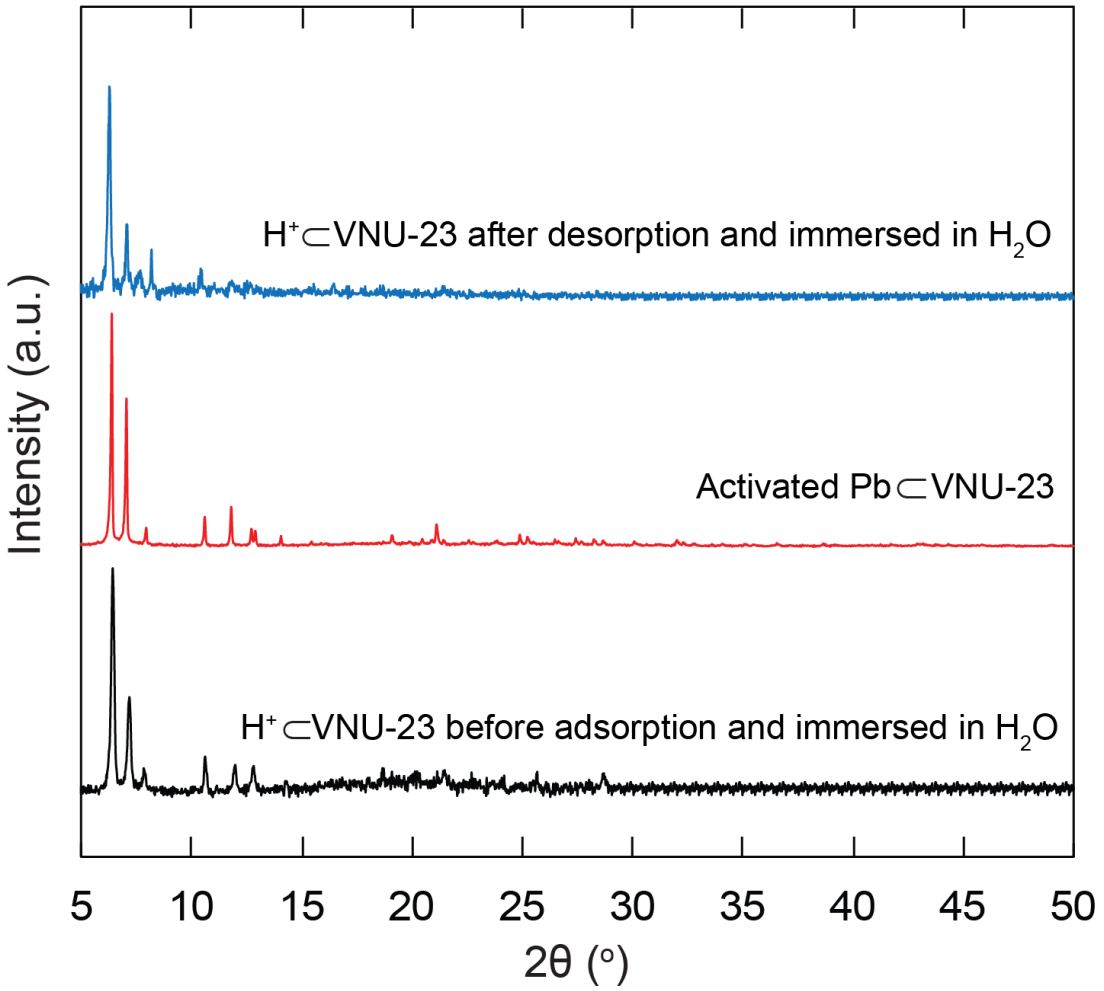

Figure S28. PXRD pattern of H^+⊂VNU-23 before adsorption of Pb^{2+} (black), and Pb⊂VNU-23 (red) as compared to the experimental pattern from the subjecting H^+⊂VNU-23 after desorption of Pb^{2+}.

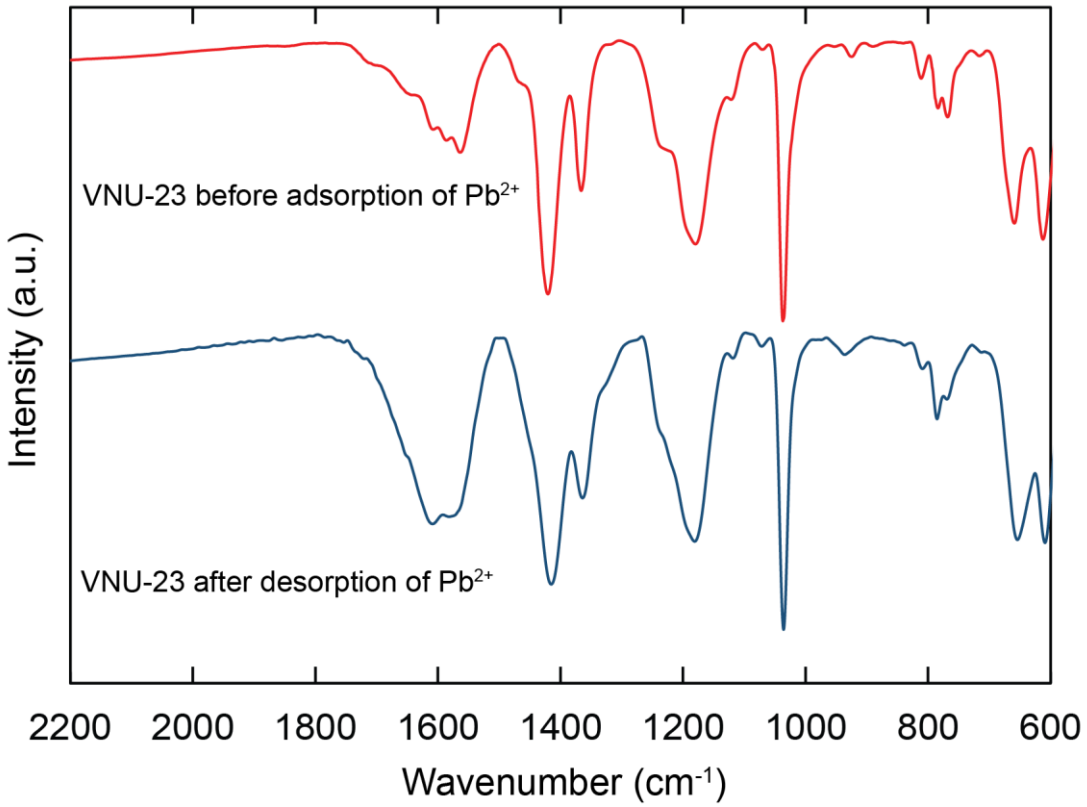

Figure S29. FT-IR spectrum of VNU-23 before adsorption of Pb^{2+} (red) in comparison with FT-IR spectrum of VNU-23 after desorption of Pb^{2+} (blue).